RESEARCH ARTICLE

NANO · MICRO small
www.small-journal.com

Advancing Glucose Sensing Through Auto-Fluorescent Polymer Brushes: From Surface Design to Nano-Arrays

Gozde Aktas Eken, Yuming Huang, Oswald Prucker, Jürgen Rühe,* and Christopher Ober**

Designing smart (bio)interfaces with the capability to sense and react to changes in local environments offers intriguing possibilities for new surface-based sensing devices and technologies. Polymer brushes make ideal materials to design such adaptive and responsive interfaces given their large variety of functional and structural possibilities as well as their outstanding abilities to respond to physical, chemical, and biological stimuli. Herein, a practical sensory interface for glucose detection based on auto-fluorescent polymer brushes decorated with phenylboronic acid (PBA) receptors is presented. The glucose-responsive luminescent surfaces, which are capable of translating conformational transitions triggered by pH variations and binding events into fluorescent readouts without the need for fluorescent dyes, are grown from both nanopatterned and non-patterned substrates. Two-photon laser scanning confocal microscopy and atomic force microscopy (AFM) analyses reveal the relationship between the brush conformation and glucose concentration and confirm that the phenylboronic acid functionalized brushes can bind glucose over a range of physiologically relevant concentrations in a reversible manner. The combination of auto-fluorescent polymer brushes with synthetic receptors presents a promising avenue for designing innovative and robust sensing systems, which are essential for various biomedical applications, among other uses.

1. Introduction

Smart interfaces, particularly those capable of sensing and responding to changes in the local environment, open up intriguing possibilities for designing novel surface-based sensing systems.[1,2] Among the promising materials for these adaptive interfaces are polymer brushes, which stand out for their functional and structural versatility, as well as their exceptional responsiveness to a wide range of physical, chemical, and biological stimuli.[3–6] Unlike bulk polymers, which often suffer from prolonged response times, these thin polymeric coatings, characterized by unique brush-like molecular arrangement, enable rapid responses without significantly altering or compromising the physical properties of underlying cores or substrates.[7] Additionally, the large surface areas provided by polymer brushes make them highly advantageous for sampling systems in biological or environmental applications. By integrating these systems with sensing and reporting motifs/entities, efficient transduction mechanisms can be facilitated, making them well-suited for use in biosensing applications.[8–10]

Functionalizing polymer brushes with synthetic receptors offers a promising strategy for imparting surfaces with target recognition and binding capabilities. One notable example of such synthetic receptors is phenylboronic acid and its derivatives which are capable of forming dynamic covalent bonds with 1,2- and 1,3-diols and have gained considerable attention for their role in the molecular recognition of mono- and polysaccharides.[11,12] These synthetic receptors have shown affinity towards various biological materials and natural products,[13] including phospholipids,[14] saccharides and polysaccharides,[15] nucleic acids,[16] metal ions,[17] and the neurotransmitter dopamine.[18] Polymers decorated with boronic acid functionalities have been widely utilized in numerous applications across different fields, such as cell profiling,[19,20] delivery systems,[21–23] responsive surfaces,[24–26] and saccharide sensors.[27,28]

Given the vital role of saccharides and related molecular species in the metabolic pathways of living organisms, detecting the presence and concentration of biologically important sugars in aqueous solutions is crucial in various medical and industrial contexts.[29] Of particular interest is the recognition of D-glucose, which has significant implications in monitoring diabetic patients—the dysregulation of D-glucose transport within the human body has been linked to diseases

G. Aktas Eken, Y. Huang, C. Ober
Materials Science and Engineering
Cornell University
Ithaca, NY 14853, USA
E-mail: ga352@cornell.edu; cko3@cornell.edu
O. Prucker, J. Rühe
Laboratory for Chemistry and Physics of Interfaces
Department of Microsystems Engineering (IMTEK)
University of Freiburg
Georges-Köhler-Allee 103, 79110 Freiburg, Germany
E-mail: ruehe@imtek.uni-freiburg.de
J. Rühe
Cluster of Excellence livMatS @FIT
Freiburg Center of Interactive Materials and Bioinspired Technologies,
University of Freiburg
Goerges-Köhler-Allee 105, 79110 Freiburg, Germany
The ORCID identification number(s) for the author(s) of this article can be found under https://doi.org/10.1002/smll.202309040

DOI: 10.1002/smll.202309040

such as cystic fibrosis, cancer, and diabetes.[30] Surface-tethered polymers containing boronic acid derivatives have emerged as compelling candidates for the development of robust sensing systems.[31] Contrary to their biological counterparts like glucose oxidase and lectins, these brush-based adaptive platforms offer fast response times, synthetic flexibility, and high tolerance to harsh conditions such as changes in pH and temperature. Various research groups have demonstrated modifications of interfaces using boronic acid-containing polymer brushes for glucose detection. For example, Sugnaux et al.[32] utilized direct surface-initiated RAFT polymerization of 3-methacrylamidophenylboronic acid to create glucose-sensitive quartz crystal microbalance with dissipation (QCM-D) sensors. Similarly, glucose-sensitive hollow-fiber membranes were prepared with phenylboronic acid functionalized poly(methacrylic acid) (PMAA) brushes, where the glucose response was evaluated via QCM-D, atomic force microscopy and flux measurements.[33] Chen et al.[34] reported the synthesis and post-polymerization modification of poly(*N*-isopropylacrylamide)-*co*-poly(acrylic acid) brushes with 3-aminophenylboronic acid (3-APBA) for glucose detection based on microcantilever deflection read-out. Despite these advances, the existing systems often rely on complex read-out processes to quantify the brush response, such as phase transitions and conformational changes induced by glucose binding, thereby limiting their practical applications. Thus, developing effective brush-based responsive platforms that allow straightforward interpretation of film responses that go beyond mere height quantification and enable real-time extraction of this information holds the potential to unlock broader prospects for their applications as point-of-care devices or implantable real-time monitoring systems.

While polymer brushes have shown considerable promise in surface-based sensing applications, their integration into miniaturized or chip-based devices has been constrained by the absence of area-specific control—the majority of the extant studies on responsive brush-based system focused on homogeneous polymer thin films formed across an entire surface, thereby forsaking the potential of nano-systems built via localized brush formation. Recent advances in nanolithography techniques have opened new avenues for investigating the role of nanoconfinement on the behavior of responsive polymer brushes. For example, Chen et al.[35] have successfully demonstrated the localized formation of solvent-responsive poly([(2-methacryloyloxy)ethyl]trimethylammonium chloride) brushes at the sub-micron scale; their finding indicated that patterned brushes provided more room for stress relaxation, thereby enhancing stability and reducing degrafting of these polyelectrolyte brushes in comparison to their non-patterned equivalent. Also, Jonas et al.[36] developed nanopatterned thermoresponsive poly(2-(2-methoxyethoxy)ethyl methacrylate) brushes and reported that such nanoconfinement has resulted in broadening and amplification of the brush response. Tagliazucchi et al.[37] modified solid-state nanochannels with pH-responsive poly(4-vinyl pyridine) brushes, showing that the conductivity of the devices was predominately influenced by the nanoscale curvature effect—the conformational changes were highly dependent on the geometry of the imposed nanoconfinement. Furthermore, the integration of different polymer brush types in a single system allows for the creation of multifunctional surfaces.[38] Huang et al.[39] have developed a mixed rod-coil brush system with poly(N-isopropylacrylamide) (PNIPAM)/poly(γ-benzyl-l-glutamate) and shown that more well-defined end-point functional nanospikes can be achieved by incorporating secondary brushes into the system. Zhao et al.[40] have reported successful fabrication of multiplexed brush architectures and reported the precise regulation of biomolecule immobilization using poly (glycidyl methacrylate)/poly(2-(2-azido-2-methyl-1-oxopropoxy) ethyl methacrylate) brush-based patterned surfaces. However, none of these studies reported the incorporation of fluorescence characteristics for optical signal transduction, a feature that would be advantageous for designing glucose-responsive devices. It is our goal to incorporate nanopatterned surfaces with fluorescent reporters to enable the potential for localized/miniaturized applications and the possibility of enhancing performance via nanoconfinement. Previously, we demonstrated that polymer brushes built from auto-fluorescent polymers can generate optical signals from pH-induced conformational changes without conventional fluorophores.[41] In this work, we extend this methodology to design and fabricate patterned glucose-responsive surfaces by integrating auto-fluorescent poly(styrene-*alt*-maleic anhydride) (pSMA) copolymer brushes with boronic acid receptors.

Herein, glucose-responsive luminescent surfaces were prepared through post-polymerization functionalization of poly(styrene-*alt*-maleic anhydride) copolymer brushes with boronic acid receptors through amine–anhydride reactions. Clusterization-triggered emission (CTE) of the resultant brushes, originating from the through-space interaction of phenyl rings and C = O groups (sub-fluorophores), enabled visualization of glucose-induced conformational changes via fluorescence microscopy. Additionally, we engineered nanopatterned brush arrays with inter-array spacings from 60 to 270 nm through an integrated process of high-resolution lithography, surface-initiated polymerization, and post-polymerization modification (PPM). These "auto-fluorescent nano-arrays," which enable fluorometric techniques to monitor polymer brush transitions in confined geometries and complex architectures at the very local scale, hold potential for medical and bioelectronic applications such as fabrication of miniaturized sensors, micro- or nanofluidic devices, and biochips, and offer advantages such as the higher density of reaction sites and much smaller sample volume.[42,43]

2. Results and Discussion

2.1. Synthesis, Nanopatterning, and Functionalization of pSMA Brushes

Beyond their intrinsic luminescence, which facilitates the conversion of conformational transitions into fluorescent readouts,[44] the choice of pSMA brushes was also guided by the reactivity of their anhydride groups, which enabled the incorporation of boronic acid receptors into the polymer structures.[45] As illustrated in **Scheme 1**, the fabrication process of the boronic acid-containing pSMA brushes comprises three steps: i) immobilization of the azo-initiator, ii) surface-initiated radical polymerization of comonomers and iii) post-polymerization modification. Details for the immobilization of the silane-based radical initiator, brush synthesis, and post-polymerization modification are provided in the experimental section. Briefly, the silicon

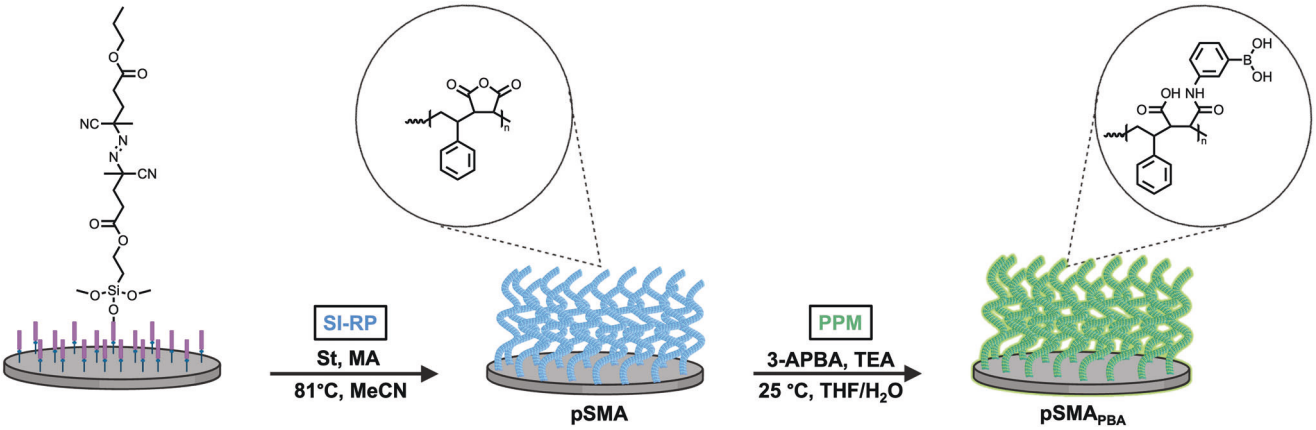

Scheme 1. Preparation of pSMA brushes through surface-initiated radical polymerization and post-polymerization modification with 3-APBA.

substrates were modified using trichlorosilane containing an azo initiator moiety from a toluene solution using triethyl amine as a catalyst. Then the brush synthesis was conducted by surface-initiated radical polymerization (SI-RP) on the initiator-modified substrates in acetonitrile at 81 °C, using equimolar amounts of styrene and maleic anhydride. Following a polymerization period of 1 h, uniform pSMA brushes with a dry thickness (h_0) of 81 ± 2 nm and a roughness of less than a few nanometers were obtained (Figure S1, Supporting Information).

Nanopatterned polymer brushes were prepared through a "bottom–up" approach using a sequence of electron beam lithography (EBL) and surface-initiated radical polymerization according to a previously reported procedure,[39] where patterns of surface-immobilized azo-initiator were prepared and used as templates to grow the brushes. (**Scheme 2**) Synthesis from the nanopatterned substrates was carried out following the same procedure as for the unstructured films which resulted in brushes with well-defined features and varying dimensions ranging from 60 to 270 nm. (**Figure 1**A,C,E,G). The slightly lower height of the nanopatterned pSMA brushes compared to homogenously grafted brush layers is attributed to the lack of lateral restraint and chain relaxation, leading to less extended chain conformations.[35,46]

The PPM of the pSMA brushes was carried out under ambient conditions. To this, the brush-modified substrates were immersed in a solution of 3-APBA in the presence of triethylamine (TEA) for varying reaction times. Under these conditions, the amine groups react readily with the anhydride moieties forming stable amide bonds. The reaction time served as a convenient parameter to regulate the degree of functionalization, which was then monitored through the thickness (equivalent to mass uptake) and composition of the modified brushes ($pSMA_{PBA}$). The brush thickness further increased up to 160 nm after the PPM as shown in **Table 1**. (Figures S2–S4, Supporting Information) Also, for the nanopatterned brushes modified with 3-APBA, the brush height increased, while no change was observed in brush morphology.

Surface composition and degree of functionalization were determined via X-ray photoelectron spectroscopy (XPS). **Figure 2**A,C present XPS survey scans recorded before and after the modification of pSMA brushes, respectively. Before modification, the survey spectrum revealed C (285 eV) and O 1s (533 eV) signals and indicated that the pSMA brushes are slightly rich in styrene content and contained ≈45 mol% of maleic anhydride, in agreement with the previously reported results.[44] Complete coverage of the silicon substrate was confirmed by the absence of any Si signal. The O1s core-level spectrum is

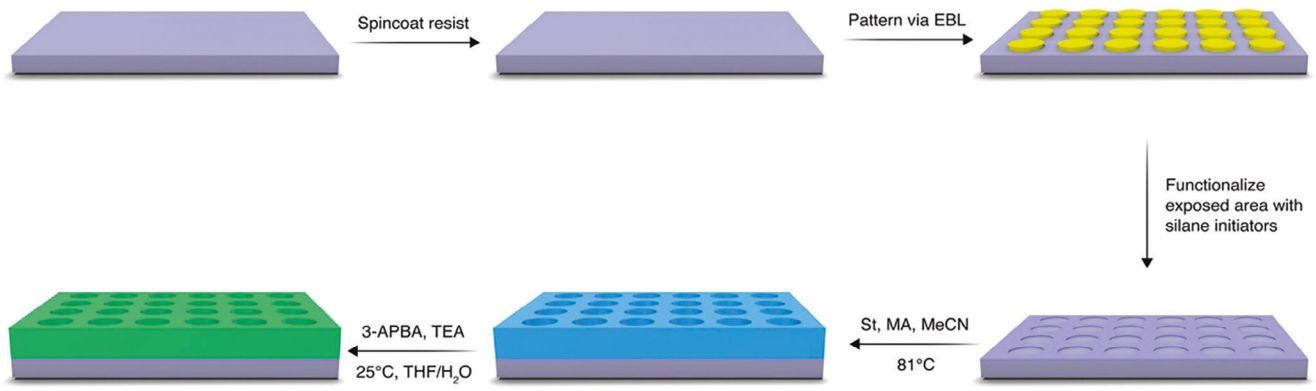

Scheme 2. Preparation of the nanopatterned brushes via electron-beam lithography, surface-initiated radical polymerization, and post-polymerization modification.

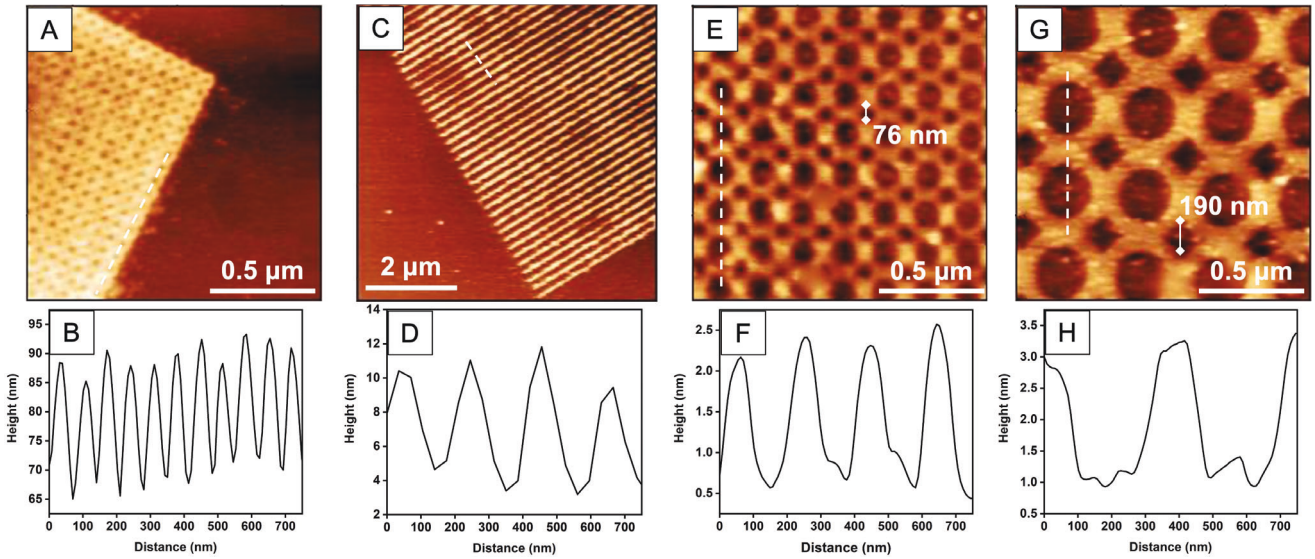

Figure 1. AFM height images and height profiles of nanopatterned pSMA brushes grown from the same substrate with different pattern designs of initiator layer. A) AFM image and B) corresponding height profile of the brushes with hollow patterns with 60 nm spacing, C) AFM image and D) corresponding height profile of the brushes with line patterns. E, G) AFM images and F, H) corresponding height profiles, of the brushes with hollow patterns with 133 and 270 nm spacings, respectively.

curve-fitted with two components with relative intensities of 1:2, which appear at 533.9 and 532.5 eV representing the etheric and the carbonyl oxygens, respectively[47] (Figure 2B). The N1s signal that appeared after modification at 400.1 eV is due to the amide bond, while the B1s signal at 191 eV confirms the presence of the boronic acid group.[33] After PPM, the O1s peak shifted to 531.8 eV as a result of the anhydride ring opening, the broad peak is deconvoluted in four components at 533.3, 532.2, 531.9, and 531.1 eV, representing oxygen atoms of boronic acid, amide, and carboxylic acid moieties. (Figure 2D)[48] The degree of functionalization of the brushes varied between 15% and 50% and reached an asymptotic value within 24 h. (Table 1; Figure S5, Supporting Information).

2.2. Fluorescence Characteristics of pSMA Brush-Based Responsive Nanoplatform

Recent developments in luminescent polymer brushes[49–51] and auto-fluorescent polymers with AIE characteristics[52,53] inspired us to engineer surfaces that can reveal real-time and localized information on brush response based on altered optical properties, effectively circumventing the challenges associated with the incorporation of conventional fluorophore labels. The intrinsic fluorescence behavior of maleic anhydride or maleimide-containing alternating copolymers was explained by a clusterization-triggered emission (CTE) mechanism in which the luminescence strongly depends on the concentration, cluster formation, and the through-space interactions of the carbonyl and the neighboring phenyl groups.[54] Aggregation of these subfluorophores into clusters induces their effective short contacts, thus promoting the overlap of intra- and intermolecular electron clouds. These interactions in turn lead to the formation of extended conjugation and stabilized molecular conformations. In the context of polymer brushes, this suggests that in the collapsed state, wherein polymer chains closely pack together, subfluorophores tend to aggregate in close proximity.[55] This arrangement facilitates the efficient overlap of n and π electrons, resulting in extended electronic conjugation and rigidified conformations, thereby inducing strong emissions. However, during the transition from collapsed to extended state, the segments of the polymer chains enter the diluted state due to hydration and electrostatic repulsion which limits intra- and interchain interactions and consequently leads to weak emissions.[41]

Table 1. Composition and thickness of the boronic acid functionalized brushes ($pSMA_{PBA}$).

Sample	Brush height [nm]	Degree of functionalization [%]
$pSMA_{PBA15}$	136 ± 6	15
$pSMA_{PBA35}$	146 ± 2	35
$pSMA_{PBA50}$	161 ± 5	50

In this study, two-photon laser scanning microscopy was used in combination with atomic force microscopy to perform fluorescence characterizations and investigate pH- and glucose-responsive behavior of the boronic acid integrated brush-based nanoplatforms. The glucose as a cis-diol reacts readily with the boronic ester through the formation of a cyclic ester.

As shown in **Figure** 3A, under two-photon excitation (λ_{ex}: 800 nm), the emission of pSMA exhibited a weak and broad peak with λ_{max} at 452 nm, corresponding to a blue fluorescence, when monitored in deionized water (DIW). Subsequent modification with 3-APBA led to an increase in the fluorescence intensity (Figure 3B–D), and the emission maxima was red-shifted to 515 nm. (Figure 3E) The enhanced fluorescence was attributed to the additional phenyl groups per repeating unit from 3-APBA, which induced the "through space" interactions with the carbonyl

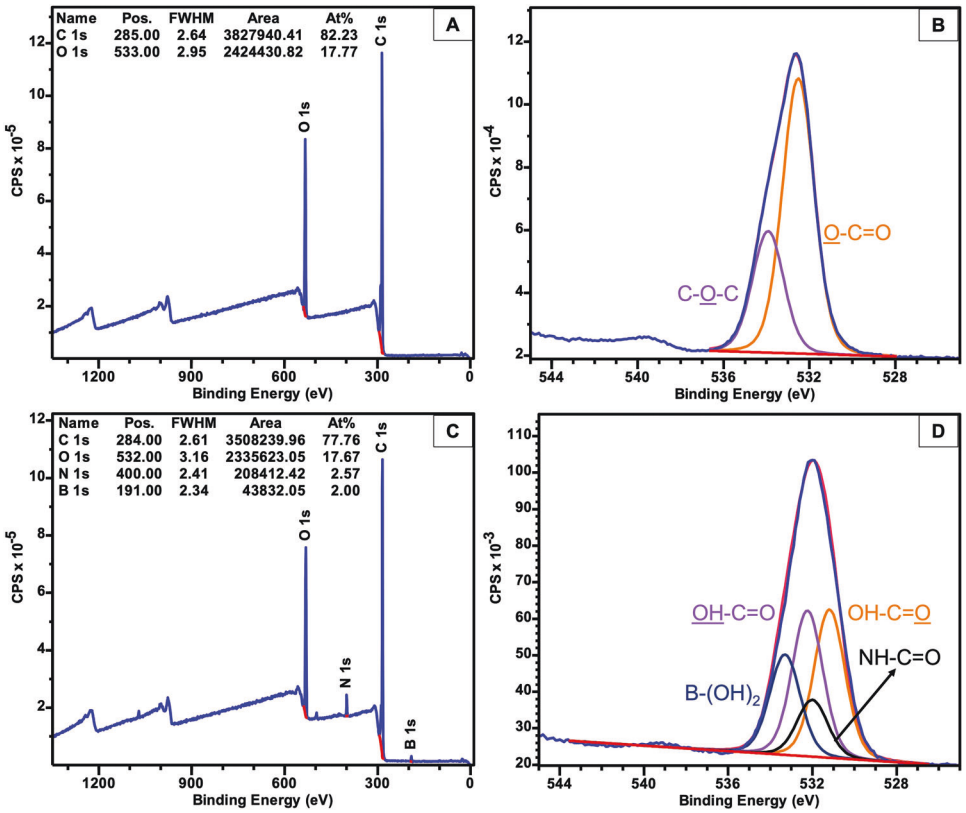

Figure 2. XPS survey spectrum of A) pSMA and C) $pSMA_{PBA50}$. High-resolution O 1s spectrum of B) pSMA and D) $pSMA_{PBA50}$.

groups in addition to the steric congestion effect.[56] This observation was further validated through the analyses of free pSMA copolymers before and after PPM with 3-APBA, which displayed enhanced fluorescence emission and a red shift in emission maxima from 482 to 516 nm in DMSO (Figure S6 and S7, Supporting Information).

Similarly, clusteroluminescence of the nanopatterned $pSMA_{PBA}$ brushes was investigated as a function of their lateral confinement in DIW by fluorescence microscopy under two-photon excitation (Figure 3F). Substrates with circular initiator patterns of varying diameters ranging from 20 to 80 nm were prepared through EBL and employed for brush growth and PPM. (Figure S8, Supporting Information) Patterns were observed to be homogeneous across the surface, and the signal intensity within the patterned areas was found to be strongly influenced by the scale and design of the patterns, which determine the steric crowding and thus the polymer chain conformation and the sub-fluorophores concentration per confined space. AFM analysis (Figure S9, Supporting Information) revealed a strong dependence of the brush height and morphology on the feature footprint size and the spacing of the initiator pattern, with a notable reduction in the maximum height of the brush nanodots accompanying the decrease in the diameter of the grafting region. 2-photon microscopy analyses illustrated that lateral confinement leads to amplification of the auto-fluorescence with cluster formation exhibiting a pronounced dependence on the lateral structure size of the nanodots. This phenomenon can be elucidated by considering the relaxation facilitated by the chains at the rim of the patterns, spreading across the surface and creating additional space for chains at the pattern center. This, in turn, led to less chain crowding, lowered height of the nanopatterned brushes, and minimized chain overlap. This relaxation effect was more pronounced as the structures became smaller but diminished for larger diameters since edge conditions weren't as influential further into the nanodots. These findings agree with the results reported earlier,[36,57-59] that described the relationship between the height of nanopatterned brushes and their lateral dimensions. In summary, the AIE characteristics of the brushes provide valuable insights into their conformation, thereby presenting a promising avenue to overcome the challenges of conventional methodologies for monitoring brush response in confined geometries.

To evaluate the pH and glucose response, $pSMA_{PBA}$ brushes were equilibrated in 0.01 M pH 9 PBS buffer and subsequently exposed to a buffer solution with 5 mM glucose. Figure 3G,H illustrate the variations in emission intensity and corresponding brush heights observed when exposing the $pSMA_{PBA}$ brushes to each solution. In DIW, phenylboronic acid exists in its neutral trigonal form and carboxylic acid groups are in the protonated state, which implies the absence of electrostatic repulsion that could counterbalance the hydrophobicity enhanced by the phenyl groups. Consequently, under these conditions, the polymer brushes tend to collapse and adopt compact structures, leading to smaller volumes. The collapsed and stiffened chains possibly contributed to the fluorescence enhancement of the brushes, as a rigid structure can restrict chain freedom and minimize

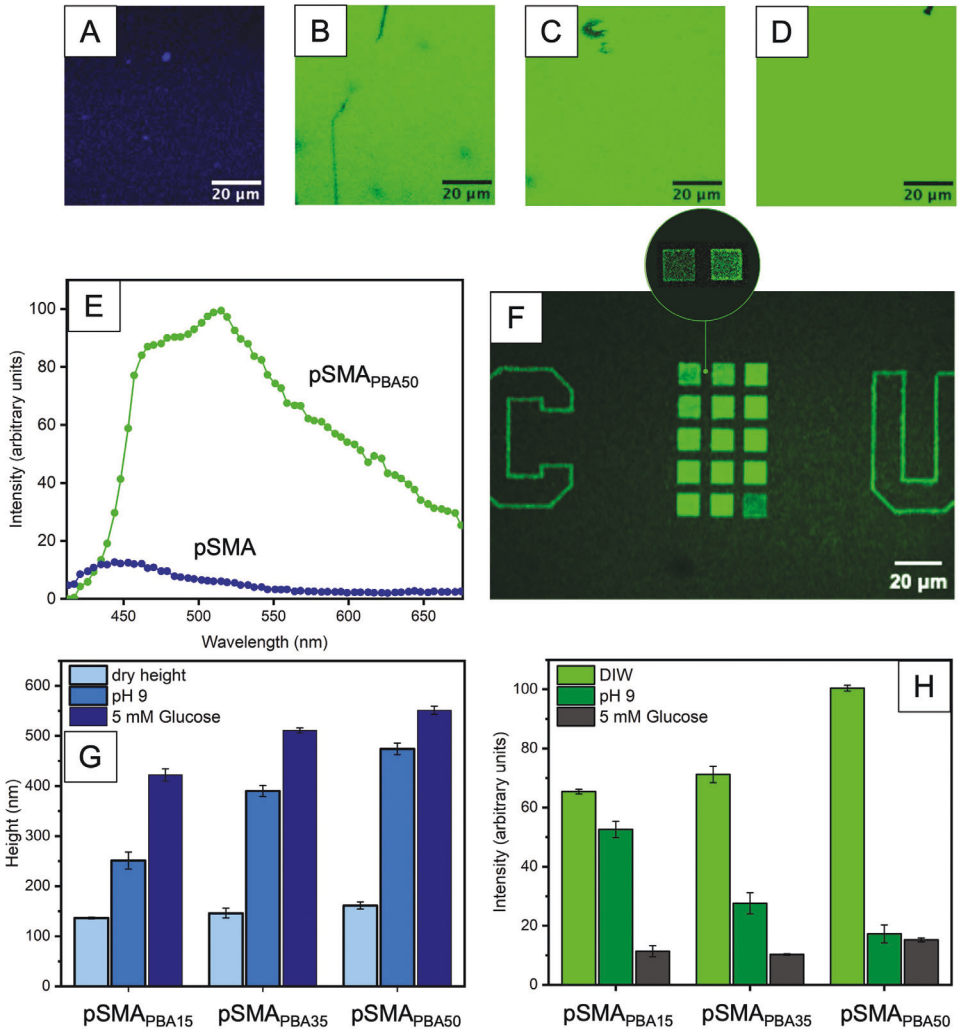

Figure 3. Fluorescence images of brush surfaces A) pSMA, B) pSMA$_{PBA15}$, C) pSMA$_{PBA35}$, D) pSMA$_{PBA50}$ recorded in DIW (collapsed state). E) Fluorescence emission spectra of the pSMA and pSMA$_{PBA50}$ polymer brush surfaces in buffer solutions collected via two-photon excitation microscopy with λ_{ex} = 800 nm. F) Fluorescence images of the nanopatterned brushes. G) The dry and swollen height of the pSMA$_{PBA}$ brushes was determined through AFM step-height measurements. H) Fluorescent intensity of the pSMA$_{PBA}$ brushes in various solutions.

nonradiative relaxation processes.[55] Upon increasing the solution pH above the pK_a of phenylboronic acid, the ionization equilibrium was shifted to the anionic tetragonal boronate acid form and induced deprotonation of carboxylic acid groups which resulted in extended and hydrated chains.[60] Subsequently, the introduction of 5 mM glucose to the incubation media further induced the formation of the boronate ester, hence enhancing the hydrophilicity and causing the brushes to swell further (**Figure 4**). Swelling of the brushes was accompanied by a decrease in fluorescence, which stems from the hydrated and highly extended state of the chains restricting intra- and inter-chain interactions and thus cluster formation.

Furthermore, combined analysis of AFM and fluorescence intensity results suggested a correlation between the change in fluorescence intensity and the swollen brush height. As shown in Figure 3G,H, the pSMA brushes functionalized ≈50% PBA (pSMA$_{PBA50}$) was found to have the maximum change in brush height from an initial dry state height of 161 to 474 nm when immersed in pH 9 buffer, subsequently reaching to 551 nm upon exposure to glucose. At the same time, based on the emission spectra, the corresponding fluorescence intensity decreased by 82% in pH 9 buffer compared to DIW, followed by a further 13% reduction upon exposure to 5 mM glucose. Such correlation suggested that factors related to the swelling of the brushes, including charge density, hydration, and steric effects, could hinder molecular clustering and hence lead to a drastic change in fluorescence intensity. However, given that blood glucose levels in healthy adults can range from 3.9 to 6.1 mM, such a limited percentage drop in fluorescence intensity upon glucose binding may pose challenges for monitoring low glucose concentrations.[30] As such, the degree of functionalization was fine-tuned to improve the sensitivity of glucose detection. As a result, a greater decrease in fluorescence intensity was found for brushes with 35% PBA (pSMA$_{PBA35}$) upon glucose exposure (62% reduction) and such decrease was further enhanced for brushes with 15% PBA (79% reduction). In summary, our findings indicated that

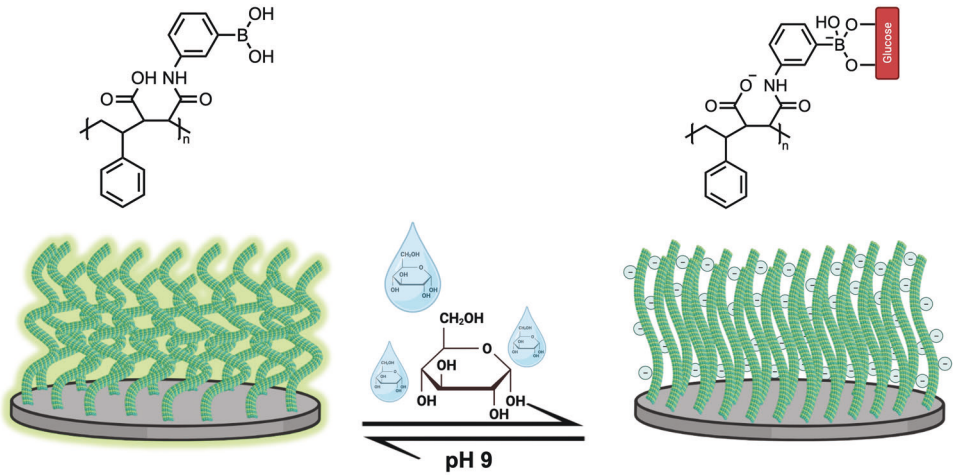

Figure 4. Schematic illustration of reversible glucose binding and glucose-triggered changes in brush conformation and luminescence.

the magnitude and sensitivity of the fluorescence response are intricately governed by the complex interplay of PBA content, hydration levels, and charge density, all of which significantly influence the cluster formation and, consequently, the fluorescence output.[61]

The impact of glucose binding on the conformation of nanopatterned brushes was also examined via in-solution AFM analysis using line patterns with 215 nm spacings. The sample was subjected to pH 9 PBS buffer, both with and without 5 mM glucose, and the resulting height change was assessed in tapping mode, as illustrated in Figure S10 (Supporting Information). The average brush height at pH 9 is ≈4.9 nm. Upon exposure to glucose, the brushes undergo a conformational transition adopting an extended conformation, swelled by a factor of 1.6 to a height of ≈7.8 nm. This suggests that the patterning does not significantly alter the glucose response and swelling behavior of $pSMA_{PBA}$ brushes.

2.3. Effect of Varying Glucose Concentration

After confirming that conformational transitions of $pSMA_{PBA}$ brushes induced by the interactions between boronic acid and glucose can be fluorometrically monitored, $pSMA_{PBA15}$ and $pSMA_{PBA35}$ were then tested over a range of glucose concentrations varying from 1 to 7 mM. In summary, fluorescence images of the modified brush surfaces were captured for visual inspection (**Figure 5**A) after equilibrating the brush samples in buffer solutions for 2 min, and emission spectra were obtained by performing lambda scans via two-photon excitation using the same excitation parameter (Figure 5B,C). The swollen brush height was measured via AFM step height measurements and plotted as a function of glucose concentration (Figure 5D,E).

As shown in Figure 5, notable reductions in fluorescence intensity are observed in conjunction with brush swelling and increasing glucose concentrations. Brush height and fluorescent intensity were highly dependent on glucose concentration for both samples. Figure 5D,E presents the change in brush thickness as a function of glucose concentration, determined via AFM step height measurements. The increase in the glucose concentration promoted the ionization of boronic acid moieties and increased the charge density of the brushes and consequently alteration in brush conformation due to enhancement in Coulombic interactions, steric crowding, and hydration. For $pSMA_{PBA15}$, the brush height exhibited a relatively linear increase, reaching up to 457 nm at a glucose concentration of ≈7 mM.; and the height of $pSMA_{PBA35}$ increased linearly up to 501 nm at 3 mM and then gradually leveled off at 544 nm. Notably, these changes in brush height were mirrored by corresponding changes in fluorescence intensity, with increased glucose concentrations resulting in diminished fluorescence emissions.

Furthermore, to assess the reversibility of glucose binding, $pSMA_{PBA35}$ was subjected to sequential exposure to a pH 9 buffer, with and without 5 mM glucose as one switching cycle. As depicted in **Figure 6**, a significant reduction in the fluorescence intensity was observed upon the exposure of glucose; the change was largely reversible in the absence of glucose. The response and swelling of the PBA-functionalized brush demonstrated almost complete reversibility over the three switching cycles.

3. Conclusion

In conclusion, this study serves as an exploration into the capabilities of $pSMA_{PBA}$ polymer brushes as sensory interfaces for glucose detection. Glucose-responsive auto-fluorescent copolymer brushes were successfully synthesized from both patterned and non-patterned substrates through surface-initiated radical polymerization and post-polymerization modification. These PBA functionalized brushes can bind glucose over a range of physiologically relevant concentrations in a reversible manner and possess the ability to convert conformational changes triggered by glucose binding into readily detectible fluorescent readouts, eliminating the necessity for adding fluorescent dyes to the analyte solutions. Two-photon laser scanning confocal microscopy and atomic force microscopy were utilized to elucidate the complex relationship between brush conformation and glucose concentration. It has been shown that the clusteroluminescence, caused by the CTE mechanism, is intricately influenced by a

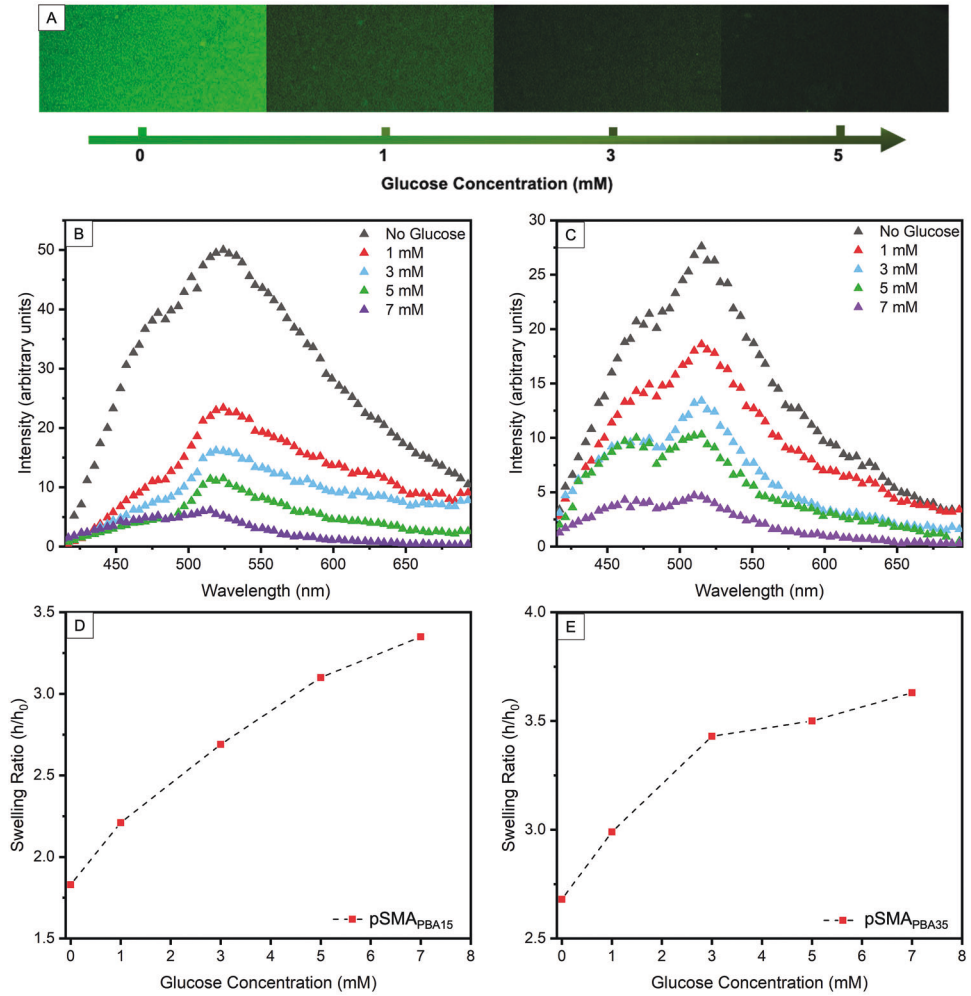

Figure 5. A) Fluorescence images of $pSMA_{PBA35}$ were recorded in buffer solutions with varying glucose concentrations. Fluorescence emission spectra of the polymer brush surfaces in buffer solutions collected via two-photon excitation microscopy with $\lambda_{ex} = 800$ nm: B) $pSMA_{PBA15}$ and C) $pSMA_{PBA35}$. Swelling ratios of D) $pSMA_{PBA15}$ and E) $pSMA_{PBA35}$ in buffer solutions with varying glucose concentrations.

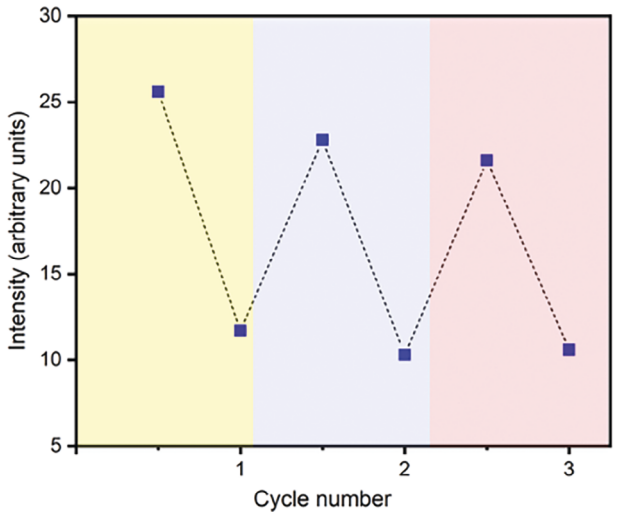

Figure 6. Alternating fluorescent intensity over three switching cycles.

variety of factors including charge density, hydration, conformational rigidity, and the nature of intra/interchain interactions present within polymers. Notably, one of the standout features of such a $pSMA_{PBA}$ brush-based sensing platform is its straightforward readout mechanism, relying on the detection of changes in fluorescence intensity in response to varying glucose concentrations. This simplicity stands in contrast to other more complex sensing approaches. Although the relatively high pK_a (≈8.8) of the PBA moiety limits its applicability for in vivo glucose monitoring and direct serum sample analysis, future efforts will concentrate on refining sensitivity and narrowing the pH response window to align more closely with physiological pH. Anticipating future advancements, the application of nanopatterned autofluorescent brushes featuring boronic acid functionalized polymers holds immense potential in medical and biological contexts, particularly in the realm of micro- or nanofluidic devices. The forthcoming focus of our investigations will delve into understanding the influence of pattern size and design on detection mechanism, efficiency, and sensitivity, thereby contributing to the further evolution of this innovative approach.

4. Experimental Section

Materials: Maleic anhydride, styrene (St), 3-aminophenylboronic acid (3-APBA), triethylamine (TEA) dicyclohexyl carbodiimide (DCC), dimethylaminopyridine (DMAP), butanol, 4,4′-azobis(4-cyanovaleric acid), tetrahydrofuran (THF) magnesium sulfate ($MgSO_4$), toluene, dimethylsulfoxide (DMSO), acetonitrile (MeCN), acetone and D-glucose were obtained from Sigma–Aldrich. 3-amino-propyldiisopropylethoxysilane (APDIPES) was purchased from Geles. Styrene was passed through an inhibitor removal column (Aldrich) before polymerization; others were used as received. A RiOs 3 water purification system was used to obtain deionized water (DIW). Silicon wafers (boron-doped, (100) orientation) were purchased from Pure Wafer.

Preparation of Initiator Functionalized Silicon Substrates: An azo-based trichlorosilane initiator was synthesized following literature procedures.[62] Substrates with the surface-immobilized asymmetric azo initiator were prepared as described below. Silicon wafers were cut into 1.5×2 cm^2 pieces and sonicated in acetone for 10 min and then dried under a nitrogen flow. Then, the substrates were exposed to oxygen plasma for 45 min. After plasma treatment, they were immersed in a solution 2 mM toluene solution of initiator containing triethylamine as a catalyst and acid scavenger. Reaction was carried out for 24 h in an inert atmosphere. Wafers were removed from the solution, washed, and then stored in the fridge.

Preparation of Patterned Substrates: Patterned substrates were prepared according to a previously reposted procedure.[39] E-beam resist was patterned via JEOL 9500, which was later used as the mask for the vapor deposition of the silane coupling agent. Prior to the deposition, the substrate was descummed via the Oxford 81 etcher to remove residual debris in the unmasked area. Vapor deposition of the silane coupling agent (APDIPES) was carried out in a closed chamber at 1 torr and 70 °C for 18 h. The substrate was cleaned with organic solvents to remove the resist mask and then transferred into a sealed flask with a 1 mM solution of mono-capped 4,4′-azobis(4-cyanovaleric acid). Subsequently, the solution was cooled to 0 °C, and 1.5 mM DCC in THF was added dropwise via syringe. The reaction was kept at 0 °C for 5 min and then allowed to warm to room temperature overnight.

Preparation of Polymer Brushes: Poly(styrene-*alt*-maleic anhydride) (pSMA) brushes were synthesized through surface-initiated radical polymerization from initiator-immobilized silicon substrates. Polymerization conditions were determined through preliminary studies. A substrate with the azo-based initiator was placed in a sealed reactor and purged with nitrogen. In a separate flask, styrene (2.3 mL, 20 mmol) and maleic anhydride (2 g, 20 mmol) were dissolved in anhydrous acetonitrile (8.0 mL) and the solution was degassed and transferred via a cannula into the reactor containing the substrate. Polymerizations were carried out at 81 °C for 1 h. After polymerization, substrates were removed from the reaction mixture, rinsed with acetonitrile, and sonicated in acetone to remove the physically adsorbed-free polymers and dried under a nitrogen flow. Then, the substrates were analyzed via AFM and XPS.

Post-polymerization Modification of pSMA Brushes with 3-APBA: PPM of pSMA brushes was conducted in diluted solutions of 3-APBA in the presence of TEA. 3-Aminophenylboronic acid (35 mg, 0.22 mmol) and triethylamine (30 µL, 0.22 mmol) were dissolved in 5.0 mL of solvent mixture that contained 90% THF and 10% DIW. Then the sample was placed in solution and the reaction was carried out for a certain amount of time. The degree of functionalization was controlled via the reaction period. After PPM substrates were cleaned and analyzed via AFM and XPS.

Atomic Force Microscopy: AFM measurements were conducted using an Oxford Instruments Cypher ES atomic force microscope equipped with an environmental scanner. Silicon tips (Oxford Instruments) with a resonance frequency of 300 kHz and a spring constant of 26 N m^{-1} were used for the dry state, while the tips with a frequency of 70 kHz and a spring constant of 2 N m^{-1} were used for in-fluid analyses. The dry and wet thickness of the brushes was measured through step-height measurements by AFM. To measure brush thickness, the samples were carefully scratched with a razor blade, and AFM height images were taken at the boundary between scratched and unscratched regions. Imaging was conducted in tapping mode, and the thickness of each sample was measured in three different regions.

XPS: XPS analyses were conducted using a Thermo Scientific Nexsa G2 X-Ray Photoelectron Spectrometer equipped with a monochromatic Al Kα high-power X-ray source operating at a power of 150 W with an emission current of 12.5 mA. The base pressure in the spectrometer was $\approx 10^{-8}$ mbar. Survey spectra (5 scans) were collected with a pass energy of 200 eV and a step size of 1 eV, and high-resolution (10 scans) ones were collected with a pass energy of 50 eV and a step size of 0.05 eV. Casa XPS software was used for data processing including fitting.

Fluorescence Measurements: Fluorescence emission spectra of free copolymer solutions were recorded using the Edinburgh FLS 1000 Spectrometer (λ_{exc} = 424 nm, d_λ = 1 nm, 435–700 nm) at RT in DMSO (8 mg mL^{-1}).

Confocal Laser Scanning Microscopy (CLSM): Fluorescence imaging of polymer brushes was performed with a confocal microscope with an inverted Axio Observer Z.1 (ZEISS LSM710). A few drops of buffer solution were added between the cover glass and the substrate, then the samples were excited with an argon laser (405 nm), and emission was collected through 63×/1.4 oil immersion objective. Images were recorded with a constant set of parameters for all samples. The two-photon excited fluorescence spectra were collected using a Zeiss LSM 880 with an excitation wavelength of 800 nm and power of 10% using a 32× water immersion objective.

Supporting Information

Supporting Information is available from the Wiley Online Library or from the author.

Acknowledgements

This study was primarily supported by the National Science Foundation through grant NSF CHE 2003588 and CHE-2304838. The authors would also like to acknowledge the Center for Research on Programmable Plant Systems (CROPPS) for the financial support with major support from the National Science Foundation under Grant No. DBI 2019674. This work made use of the Cornell Center for Materials Research Shared Facilities, which is supported through the NSF MRSEC program (DMR-1719875) and CESI Shared Facilities partly sponsored by the NSF MRI DMR-1338010 and Kavli Institute at Cornell and the Cornell NanoScale Facility, a member of the National Nanotechnology Coordinated Infrastructure (NNCI), which is supported by the National Science Foundation (Grant NNCI-2025233). The fluorescence characterizations made use of the Imaging facilities in Biotechnology Resource Center (BRC) at the Cornell Institute of Biotechnology (RRID:SCR_021741), with NYSTEM (C029155) and NIH (S10OD018516) funding for the shared Zeiss LSM880 confocal/multiphoton microscope and with NIH 1S10RR025502 funding for the shared Zeiss LSM 710 Confocal Microscope. This work was partially funded through the Cluster of Excellence Living, Adaptive, and Energy-autonomous Materials Systems (*liv*MatS) by the Deutsche Forschungsgemeinschaft (German Research Foundation) under Germany's Excellence Strategy EXC-2193/1-390951807. Support by the Research Cluster "Interactive and Programmable Materials (IPROM)" funded by the Carl Zeiss Foundation is gratefully acknowledged.

Conflict of Interest

The authors declare no conflict of interest.

Author Contributions

G.A.E. and Y.H. contributed equally to this work. The manuscript was written through the contributions of all authors. All authors have given approval to the final version of the manuscript.

Data Availability Statement

The data that support the findings of this study are available on request from the corresponding author. The data are not publicly available due to privacy or ethical restrictions.

Keywords

boronic acid, glucose sensing, luminescent surfaces, nanopatterned polymer brushes, smart interfaces

Received: October 8, 2023
Revised: December 23, 2023
Published online:

[1] C. Barner-Kowollik, A. S. Goldmann, F. H. Schacher, *Macromolecules* **2016**, *49*, 5001.
[2] M. E. Welch, C. K. Ober, *J. Polym. Sci., Part B: Polym. Phys.* **2013**, *51*, 1457.
[3] W.-L. Chen, R. Cordero, H. Tran, C. K. Ober, *Macromolecules* **2017**, *50*, 4089.
[4] S. Ma, X. Zhang, B. Yu, F. Zhou, *NPG Asia Mater.* **2019**, *11*, 24.
[5] M. A. Stuart, W. T. Huck, J. Genzer, M. Müller, C. Ober, M. Stamm, G. B. Sukhorukov, I. Szleifer, V. V. Tsukruk, M. Urban, F. Winnik, S. Zauscher, I. Luzinov, S. Minko, *Nat. Mater.* **2010**, *9*, 101.
[6] J. Rühe, *Polymer Brushes: Synthesis, Characterization and Applications*, Wiley-VCH, Weinheim, Germany **2004**, pp. 1–31.
[7] D. Li, L. Xu, J. Wang, J. E. Gautrot, *Adv. Healthcare Mater.* **2021**, *10*, 2000953.
[8] G. C. Ritsema van Eck, L. Chiappisi, S. de Beer, *ACS Appl Polym Mater* **2022**, *4*, 3062.
[9] T. Chen, R. Ferris, J. Zhang, R. Ducker, S. Zauscher, *Progr. Polym. Sci.* **2010**, *35*, 94.
[10] Q. A. Besford, C. Rossner, A. Fery, *Adv. Funct. Mater.* **2023**, *33*, 2214915.
[11] A. Schiller, in *Molecules at Work: Selfassembly, Nanomaterials, Molecular Machinery*, Wiley-VCH, Weinheim, Germany **2012**, pp. 315–338.
[12] K. Lacina, P. Skládal, T. D. James, *Chem. Cent. J.* **2014**, *8*, 60.
[13] S. D. Bull, M. G. Davidson, J. M. H. van den Elsen, J. S. Fossey, A. T. A. Jenkins, Y.-B. Jiang, Y. Kubo, F. Marken, K. Sakurai, J. Zhao, T. D. James, *Acc. Chem. Res.* **2013**, *46*, 312.
[14] L. H. Mak, S. N. Georgiades, E. Rosivatz, G. F. Whyte, M. Mirabelli, R. Vilar, R. Woscholski, *ACS Chem. Biol.* **2011**, *6*, 1382.
[15] W. J. Ramsay, H. Bayley, *Angew. Chem., Int. Ed.* **2018**, *57*, 2841.
[16] J. H. Lee, A. R. Jeong, J.-H. Jung, C.-M. Park, J.-I. Hong, *J. Org. Chem.* **2011**, *76*, 417.
[17] X. Wu, X.-X. Chen, Y.-B. Jiang, *Analyst* **2017**, *142*, 1403.
[18] P. L. Fosso Tene, A. Weltin, F. Tritz, H. J. Defeu Soufo, T. Brandstetter, J. Rühe, *Langmuir* **2021**, *37*, 11041.
[19] M. Jiang, A. N. Chattopadhyay, C. H. Li, Y. Geng, D. C. Luther, R. Huang, V. M. Rotello, *Chem. Sci.* **2022**, *13*, 12899.
[20] A. E. Ivanov, J. Eccles, H. A. Panahi, A. Kumar, M. V. Kuzimenkova, L. Nilsson, B. Bergenståhl, N. Long, G. J. Phillips, S. V. Mikhalovsky, I. Y. Galaev, B. Mattiasson, *J. Biomed. Mater. Res., Part A* **2009**, *88A*, 213.
[21] Ł. Banach, G. T. Williams, J. S. Fossey, *Adv. Ther.* **2021**, *4*, 2100118.
[22] G. Vancoillie, R. Hoogenboom, *Sensors* **2016**, *16*, 1736.
[23] M. Taleb, Y. Ding, B. Wang, N. Yang, X. Han, C. Du, Y. Qi, Y. Zhang, Z. F. Sabet, H. R. Alanagh, A. Mujeeb, K. Khajeh, G. Nie, *Adv. Healthcare Mater.* **2019**, *8*, 1900283.
[24] L. Song, J. Zhao, S. Luan, J. Ma, J. Liu, X. Xu, J. Yin, *ACS Appl. Mater. Interfaces* **2013**, *5*, 13207.
[25] H. Liu, Y. Li, K. Sun, J. Fan, P. Zhang, J. Meng, S. Wang, L. Jiang, *J. Am. Chem. Soc.* **2013**, *135*, 7603.
[26] S. Lamping, T. Otremba, B. J. Ravoo, *Angew. Chem., Int. Ed.* **2018**, *57*, 2474.
[27] M. Elsherif, M. U. Hassan, A. K. Yetisen, H. Butt, *ACS Nano* **2018**, *12*, 2283.
[28] F. S. H. Krismastuti, W. L. A. Brooks, M. J. Sweetman, B. S. Sumerlin, N. H. Voelcker, *J. Mater. Chem. B* **2014**, *2*, 3972.
[29] W. Zhai, X. Sun, T. D. James, J. S. Fossey, *Chem Asian J* **2015**, *10*, 1836.
[30] B. Giri, S. Dey, T. Das, M. Sarkar, J. Banerjee, S. K. Dash, *Biomed. Pharmacother.* **2018**, *107*, 306.
[31] S. Hajizadeh, B. Mattiasson, in *Polymer and Biopolymer Brushes*, Wiley-VCH, Weinheim, Germany **2017**, pp. 479–496.
[32] C. Sugnaux, H.-A. Klok, *Macromol. Rapid Commun.* **2014**, *35*, 1402.
[33] N. Fortin, H.-A. Klok, *ACS Appl. Mater. Interfaces* **2015**, *7*, 4631.
[34] T. Chen, D. P. Chang, T. Liu, R. Desikan, R. Datar, T. Thundat, R. Berger, S. Zauscher, *J. Mater. Chem.* **2010**, *20*, 3391.
[35] W.-L. Chen, M. Menzel, T. Watanabe, O. Prucker, J. Rühe, C. K. Ober, *Langmuir* **2017**, *33*, 3296.
[36] A. M. Jonas, Z. Hu, K. Glinel, W. T. S. Huck, *Nano Lett.* **2008**, *8*, 3819.
[37] M. Tagliazucchi, O. Azzaroni, I. Szleifer, *J. Am. Chem. Soc.* **2010**, *132*, 12404.
[38] Z. Xie, T. Gan, L. Fang, X. Zhou, *Soft Matter* **2020**, *16*, 8736.
[39] Y. Huang, H. Tran, C. K. Ober, *ACS Macro Lett.* **2021**, *10*, 755.
[40] H. Zhao, T. Chen, T. Wu, L. Xie, Y. Ma, J. Sha, *Biomater Adv* **2022**, *141*, 213092.
[41] G. Aktas Eken, Y. Huang, Y. Guo, C. Ober, *ACS Appl Polym Mater* **2023**, *5*, 1613.
[42] Q. Yu, L. K. Ista, R. Gu, S. Zauscher, G. P. López, *Nanoscale* **2016**, *8*, 680.
[43] A. Rastogi, M. Y. Paik, M. Tanaka, C. K. Ober, *ACS Nano* **2010**, *4*, 771.
[44] W. Guo, L. Xiong, C. M. Reese, D. V. Amato, B. J. Thompson, P. K. Logan, D. L. Patton, *Polym. Chem.* **2017**, *8*, 6778.
[45] Y. Ru, X. Zhang, W. Song, Z. Liu, H. Feng, B. Wang, M. Guo, X. Wang, C. Luo, W. Yang, Y. Li, J. Qiao, *Polym. Chem.* **2016**, *7*, 6250.
[46] A. M. Jonas, Z. Hu, K. Glinel, W. T. S. Huck, *Macromolecules* **2008**, *41*, 6859.
[47] H. Y. Mun, H. C. Jeong, J. H. Lee, J. H. Won, H. G. Park, B. Y. Oh, D. S. Seo, *RSC Adv.* **2016**, *6*, 76743.
[48] A. Artemenko, A. Shchukarev, P. Štenclová, T. Wågberg, J. Segervald, X. Jia, A. Kromka, *IOP Conf Ser Mater Sci Eng* **2021**, *1050*, 012001.
[49] J. Poisson, Z. M. Hudson, *Chem. Eur. J.* **2022**, *28*, 202200552.
[50] Q. A. Besford, P. Uhlmann, A. Fery, *Macromol. Chem. Phys.* **2023**, *224*, 2200180.
[51] J. Bünsow, J. Erath, P. M. Biesheuvel, A. Fery, W. T. S. Huck, *Angew. Chem., Int. Ed.* **2011**, *50*, 9629.
[52] K. Bauri, B. Saha, A. Banerjee, P. De, *Polym. Chem.* **2020**, *11*, 7293.
[53] Z. Guo, Y. Ru, W. Song, Z. Liu, X. Zhang, J. Qiao, *Macromol. Rapid Commun.* **2017**, *38*, 1700099.
[54] W. Zhang Yuan, Y. Zhang, *J. Polym. Sci., Part A: Polym. Chem.* **2017**, *55*, 560.
[55] H. Zhang, Z. Zhao, P. R. McGonigal, R. Ye, S. Liu, J. W. Y. Lam, R. T. K. Kwok, W. Z. Yuan, J. Xie, A. L. Rogach, B. Z. Tang, *Mater. Today* **2020**, *32*, 275.
[56] J. Huang, X. Geng, C. Peng, T. Z. Grove, S. R. Turner, *Macromol. Rapid Commun.* **2018**, *39*, 1700530.
[57] W.-K. Lee, M. Patra, P. Linse, S. Zauscher, *Small* **2007**, *3*, 63.
[58] S. J. Ahn, M. Kaholek, W.-K. Lee, B. LaMattina, T. H. LaBean, S. Zauscher, *Adv. Mater.* **2004**, *16*, 2141.
[59] M. Kaholek, W.-K. Lee, J. Feng, B. LaMattina, D. J. Dyer, S. Zauscher, *Chem. Mater.* **2006**, *18*, 3660.
[60] G. Vancoillie, R. Hoogenboom, *Polym. Chem.* **2016**, *7*, 5484.
[61] P. Liao, J. Huang, Y. Yan, B. Z. Tang, *Mater. Chem. Front.* **2021**, *5*, 6693.
[62] D. L. Patton, K. A. Page, C. Xu, K. L. Genson, M. J. Fasolka, K. L. Beers, *Macromolecules* **2007**, *40*, 6017.